Inhibition of MALT1 Decreases Neuroinflammation and Pathogenicity of Virulent Rabies Virus in Mice

E. Kip,[a,b,c] J. Staal,[b,c] H. G. Tima,[d] L. Verstrepen,[b,c] M. Romano,[d] K. Lemeire,[b,c] V. Suin,[a] A. Hamouda,[a] M. Baens,[e] C. Libert,[b,c] M. Kalai,[a*] S. Van Gucht,[a,f] R. Beyaert[b,c]

[a]National Reference Center of Rabies, Viral diseases, Infectious Diseases in Humans, Sciensano, Brussels, Belgium
[b]Center for Inflammation Research, VIB, Ghent, Belgium
[c]Department of Biomedical Molecular Biology, Ghent University, Ghent, Belgium
[d]Scientific Service Immunology, Infectious Diseases in Humans, Sciensano, Brussels, Belgium
[e]Centre for Drug Design and Discovery (CD3), Leuven, Belgium
[f]Laboratory of Virology, Department of Virology, Parasitology and Immunology, Faculty of Veterinary Medicine, Ghent University, Ghent, Belgium

ABSTRACT Rabies virus is a neurovirulent RNA virus, which causes about 59,000 human deaths each year. Treatment for rabies does not exist due to incomplete understanding of the pathogenesis. MALT1 mediates activation of several immune cell types and is involved in the proliferation and survival of cancer cells. MALT1 acts as a scaffold protein for NF-κB signaling and a cysteine protease that cleaves substrates, leading to the expression of immunoregulatory genes. Here, we examined the impact of genetic or pharmacological MALT1 inhibition in mice on disease development after infection with the virulent rabies virus strain CVS-11. Morbidity and mortality were significantly delayed in $Malt1^{-/-}$ compared to $Malt1^{+/+}$ mice, and this effect was associated with lower viral load, proinflammatory gene expression, and infiltration and activation of immune cells in the brain. Specific deletion of $Malt1$ in T cells also delayed disease development, while deletion in myeloid cells, neuronal cells, or NK cells had no effect. Disease development was also delayed in mice treated with the MALT1 protease inhibitor mepazine and in knock-in mice expressing a catalytically inactive MALT1 mutant protein, showing an important role of MALT1 proteolytic activity. The described protective effect of MALT1 inhibition against infection with a virulent rabies virus is the precise opposite of the sensitizing effect of MALT1 inhibition that we previously observed in the case of infection with an attenuated rabies virus strain. Together, these data demonstrate that the role of immunoregulatory responses in rabies pathogenicity is dependent on virus virulence and reveal the potential of MALT1 inhibition for therapeutic intervention.

IMPORTANCE Rabies virus is a neurotropic RNA virus that causes encephalitis and still poses an enormous challenge to animal and public health. Efforts to establish reliable therapeutic strategies have been unsuccessful and are hampered by gaps in the understanding of virus pathogenicity. MALT1 is an intracellular protease that mediates the activation of several innate and adaptive immune cells in response to multiple receptors, and therapeutic MALT1 targeting is believed to be a valid approach for autoimmunity and MALT1-addicted cancers. Here, we study the impact of MALT1 deficiency on brain inflammation and disease development in response to infection of mice with the highly virulent CVS-11 rabies virus. We demonstrate that pharmacological or genetic MALT1 inhibition decreases neuroinflammation and extends the survival of CVS-11-infected mice, providing new insights in the biology of MALT1 and rabies virus infection.

KEYWORDS CVS-11, MALT1, neuroinflammation, rabies pathogenesis, rabies virus

Rabies virus is a highly neurotropic negative single-stranded RNA virus that causes a lethal infection of the brain (1). Although human rabies disease has been controlled in developed countries by dog vaccination (2), wildlife vaccination, and proper postexposure prophylaxis, in developing countries the virus still kills at least 59,000 humans each year because of inadequate control of rabies in domestic dog populations. Although the death rate can be lowered substantially through the use of effective postexposure prophylaxis for victims of rabid-animal bites, which involves a course of vaccination and immunoglobulin administered immediately after exposure, high costs and the frequent lack of rabies vaccine in developing countries remain a problem. Specific treatment for disease does not exist due to incomplete understanding of the pathogenesis (3). Upon onset of disease, rabies has the highest case fatality rate of any infectious disease (4), making human rabies an important public health problem.

When a pathogen enters the central nervous system (CNS), an immediate innate immune response is initiated. The immune response, aimed at the clearance of the pathogen and protection, may also lead to destruction of the CNS structure (5). Rabies virus infection can be detected by Toll-like receptor 3 (TLR3), retinoic inducible gene I (RIG-I)-like receptors, and melanoma differentiation-associated protein 5 (MDA-5), which are present in neuronal cells and glial cells (6–8). This triggers classical type I interferon (IFN), chemoattractive, and inflammatory responses in infected cells (9, 10). Consequently, activation of receptors on macrophages and glial cells induces in turn the secretion of several other cytokines and chemokines and further leads to the upregulation of major histocompatibility complex by microglia and to increased expression of adhesion molecules (CXCL10) that can modulate the trafficking of T cells to the CNS (5).

Rabies viruses can evade the host immune system, resulting in failure to clear the virus from the brain (11, 12). Although an inflammatory response in the early stage of infection is important for the clearance of rabies virus from the brain (13), there is no evidence that severe inflammation in the late stage is beneficial to fight the disease. In many cases, the virus does not destroy neurons directly but may cause indirect damage by triggering a cell-mediated immune response within the CNS (14, 15). Still, the mechanisms involved in CNS dysfunction following infection with neurotropic viruses are not fully understood.

CVS-11 is a mouse-adapted laboratory-fixed rabies virus challenge standard strain. It is widely used for the study of rabies pathogenesis because it shows a strong neurotropism in experimental animals (16–18) and the mortality curves following intranasal inoculation are highly reproducible (19). Intranasal inoculation of a low dose of CVS-11 quickly leads to brain invasion and infection and causes fatal encephalitis. CVS-11 is usually less immunogenic and presents a higher tropism for the CNS than attenuated strains of rabies virus (16).

MALT1 (mucosa-associated lymphoid tissue lymphoma translocation gene 1) is an intracellular protein that mediates nuclear factor κB (NF-κB) and p38/JNK mitogen-activated protein (MAP) kinase signaling in response to many stimuli, such as antigen receptor activation in lymphocytes, dectin-driven dendritic cell activation, and thrombin- and angiotensin-induced activation of fibroblasts and endothelial cells. In unstimulated cells, MALT1 is constitutively bound to the caspase recruitment domain (CARD)-containing protein BCL10 in the cytoplasm. Upon stimulation, MALT1/BCL10 binds to another CARD-containing protein: CARD11 (also known as CARMA1), CARD9, CARD10 (also known as CARMA3), or CARD14 (also known as CARMA2), depending on the cell type (20). Formation of the CARD-BCL10-MALT1 (CBM) complex leads to the recruitment of other signaling proteins, which mediate activation of IκB kinase (IKK) and p38/JNK MAP kinases, culminating in the activation of NF-κB and other transcription factors (21). NF-κB drives the expression of many genes leading to cytokine expression and inflammatory and immune cell activation/proliferation and survival. Moreover, MALT1 is constitutively activated in certain cancers due to chromosomal translocation of MALT1 and overexpression or oncogenic mutation in upstream signaling molecules, contrib-

uting to cancer cell proliferation and survival (22, 23). Importantly, in addition to its scaffold function, MALT1 has proteolytic activity that allows it to cleave specific substrates such as NF-κB family members (24), ubiquitin-regulatory proteins (25–27), and RNase- and mRNA-destabilizing proteins (28, 29), which can further fine-tune inducible gene expression and contributes to cell activation and proliferation (reviewed in reference 30).

$Malt1^{-/-}$ mice are viable and fertile and were first described in references 31 and 32. The total number of T cells and the distribution of CD4 and CD8 cells in the spleen, lymph nodes, and thymus are comparable in $Malt1^{+/+}$ and $Malt1^{-/-}$ mice, but absence of MALT1 is associated with decreased T cell activation, proliferation, and interleukin-2 (IL-2) production (32). $Malt1^{-/-}$ mice also present a reduced number of marginal zone B cells and B1 cells, impaired IgM- and CD40-induced proliferation, and lower basal serum immunoglobulin levels, especially IgM and IgG3. These effects are also seen in MALT1 knock-in mice expressing a catalytically inactive point mutant of MALT1 in which the scaffold function is retained. Notably, protease-dead (PD) MALT1 knock-in mice show a deregulated effector T-cell response, leading to spontaneous autoimmunity (reviewed in reference 33). In contrast, inhibition of MALT1 using small-compound inhibitors is not associated with autoimmunity, which may reflect temporal or dose-dependent effects of MALT1 inhibition. Therefore, inhibition of MALT1 protease activity by small inhibitors is currently of high therapeutic interest for autoimmune diseases and certain cancers. In this context, promising results were already reported in preclinical mouse models of multiple sclerosis (34, 35), rheumatoid arthritis (36), immune thrombocytopenia (37), and diffuse large B cell lymphoma (38, 39).

Here, we studied the role of MALT1 in rabies virus infection, inflammation, and disease. In order to gain better insight on the pathogenesis of rabies and the role of MALT1 in neuroinflammation, we inoculated the highly virulent rabies strain CVS-11 intranasally to wild-type mice, MALT1 knockout ($Malt^{-/-}$) mice, conditional knockout mice lacking MALT1 in specific cell types, MALT1 protease-dead knock-in mice, or mepazine-treated wild-type mice.

RESULTS

Morbidity and mortality are delayed in $Malt1^{-/-}$ mice after CVS-11 infection. Intranasal inoculation of CVS-11 in wild-type $Malt1^{+/+}$ mice led to fatal encephalitis. Mice developed the first clinical signs at 6 days postinoculation (dpi) (Fig. 1A and C) and had to be euthanized at 8 dpi, because they reached the endpoint of the disease (score 7). CVS-11-infected MALT1$^{-/-}$ mice developed the first clinical signs at 8 dpi (Fig. 1A) and had to be euthanized (score 7) from 9 to 18 dpi (Fig. 1B). Their median survival time was 12 days. A mortality rate of 100% was observed in $Malt1^{+/+}$ and $Malt1^{-/-}$ mice, but $Malt1^{-/-}$ mice survived 1 to 10 days longer than $Malt1^{+/+}$ mice (Fig. 1B). These results suggest that MALT1 contributes to the pathogenesis and clinical signs caused by the virulent rabies strain CVS-11.

MALT1 deficiency slows down virus infection in the brain. Virus infection was monitored by measuring viral RNA loads and tissue staining for N proteins (fluorescent antigen test [FAT]) and G proteins (immunohistochemistry [IHC]) at 4 and 8 dpi in $Malt1^{-/-}$ and $Malt1^{+/+}$ mice (Fig. 2A). Viral RNA loads were analyzed in total brain, olfactory bulbs, cerebrum, and cerebellum by real-time quantitative reverse transcriptase PCR (RT-qPCR). At 4 dpi (incubation period), viral RNA loads were significantly lower in total brain, olfactory bulbs, cerebrum, and diencephalon of $Malt1^{-/-}$ mice than $Malt1^{+/+}$ mice (Fig. 2B and C). At the late stage of infection (8 dpi), the amount of virus in the brain had increased in both $Malt1^{-/-}$ and $Malt1^{+/+}$ brains. No significant differences could be observed anymore in total brains between $Malt1^{-/-}$ and $Malt1^{+/+}$ mice (Fig. 2B), except for a slight, but significantly lower RNA load in the cerebellum of MALT1$^{-/-}$ brains (Fig. 2D).

Fluorescence staining of the N protein yielded a similar signal in $Malt1^{-/-}$ and $Malt1^{+/+}$ mouse brains at 8 dpi, whereas no staining could be detected at 4 dpi (Fig. 2E). Immunohistochemical staining of the G protein gave similar results in $Malt1^{-/-}$
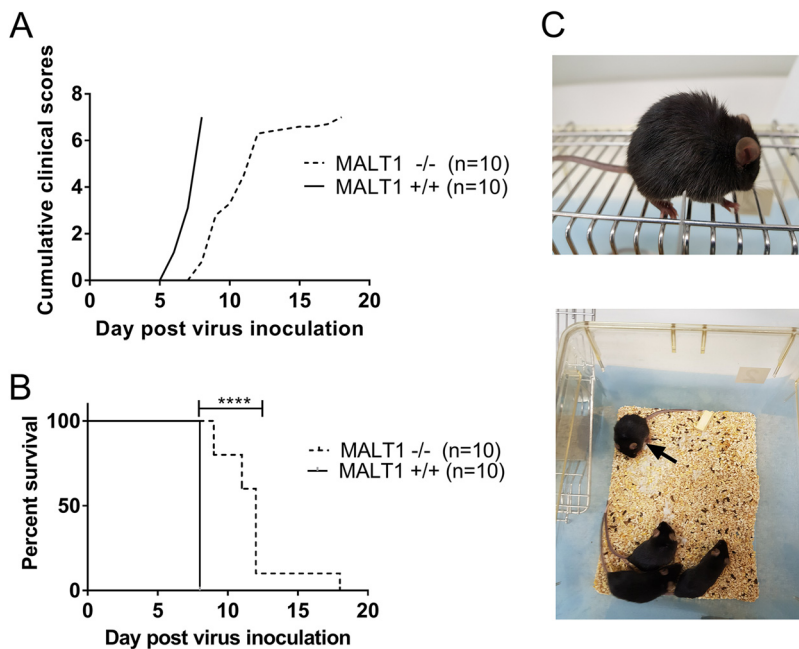
FIG 1 MALT1 deficiency delays morbidity caused by CVS-11. $Malt1^{-/-}$ ($n = 10$) and $Malt1^{+/+}$ ($n = 10$) littermates were infected intranasally with CVS-11 virus. (A, B) Cumulative clinical signs (A) and survival rates (B) were assessed. All $Malt1^{-/-}$ and $Malt1^{+/+}$ mice developed severe disease and had to be euthanized. $Malt1^{-/-}$ mice developed the first symptoms later than $Malt1^{+/+}$ mice and had to be sacrificed 2 to 10 days later than the $Malt1^{+/+}$ mice. Results are representative of two independent experiments. (C) Typical disease signs observed in a rabid mouse: rough hair coat, paralysis, isolation from the group.

and $Malt1^{+/+}$ brains at 8 dpi (Fig. 2F). The G protein was detected in Purkinje cells in the cerebellum, pyramidal cells of the hippocampus, and cortical cells of the cerebrum in both $Malt1^{+/+}$ and $Malt1^{-/-}$ mice. No staining could be observed at 4 dpi (data not shown). Together, these data demonstrate that MALT1 deficiency reduces viral load in the brain of infected mice during the incubation phase.

Inflammatory gene expression is disrupted in the brain of $Malt1^{-/-}$ mice. Immune responses and inflammation of the brain were assessed by determining the levels of mRNAs specific for type II interferons (gamma interferon [IFN-γ]), proinflammatory cytokines (tumor necrosis factor [TNF], IL-1β, IL-6), inflammasome activation (caspase-1, NLRP3), chemokines (MCP1, CXCL10), microglia activation (A1), T cell markers (CD8 and CD4), and inducible nitric oxide synthase (iNOS) enzyme in the brain. In general, all investigated genes were upregulated following CVS-11 infection in wild-type mice compared to the corresponding uninfected controls. At 4 dpi, expression of TNF and CXCL10 was significantly lower in $Malt1^{-/-}$ brains than in $Malt1^{+/+}$ brains (Fig. 3). At 8 dpi, expression of IFN-γ, IL-1β, IL-6, NLRP3, caspase-1, A1, CD8, and iNOS was also significantly lower in $Malt1^{-/-}$ brains. Decreased expression of CD8 and IFN-γ suggests a defective cytotoxic T-cell response. Decreased IFN-γ can also indicate a defective NK/NKT cell response. Reduced proinflammatory cytokine expression and reduced expression of the marker of microglial cell activation A1 also indicate a lower neuroinflammation in the brain of $Malt1^{-/-}$ mice than in that of wild-type mice. These results suggest that several inflammatory and immune responses are disrupted in $Malt1^{-/-}$ mice.

MALT1 deficiency impairs inflammatory and immune cell activation and infiltration. To investigate if the above-described defects in virus-induced cytokine and chemokine gene expression in $Malt1^{-/-}$ mice were also associated with an altered recruitment and activation of inflammatory cells, immunohistological and flow cytometric analysis for different inflammatory cell markers was performed on brain sections from infected $Malt1^{+/+}$ and $Malt1^{-/-}$ mice in comparison to phosphate-buffered saline
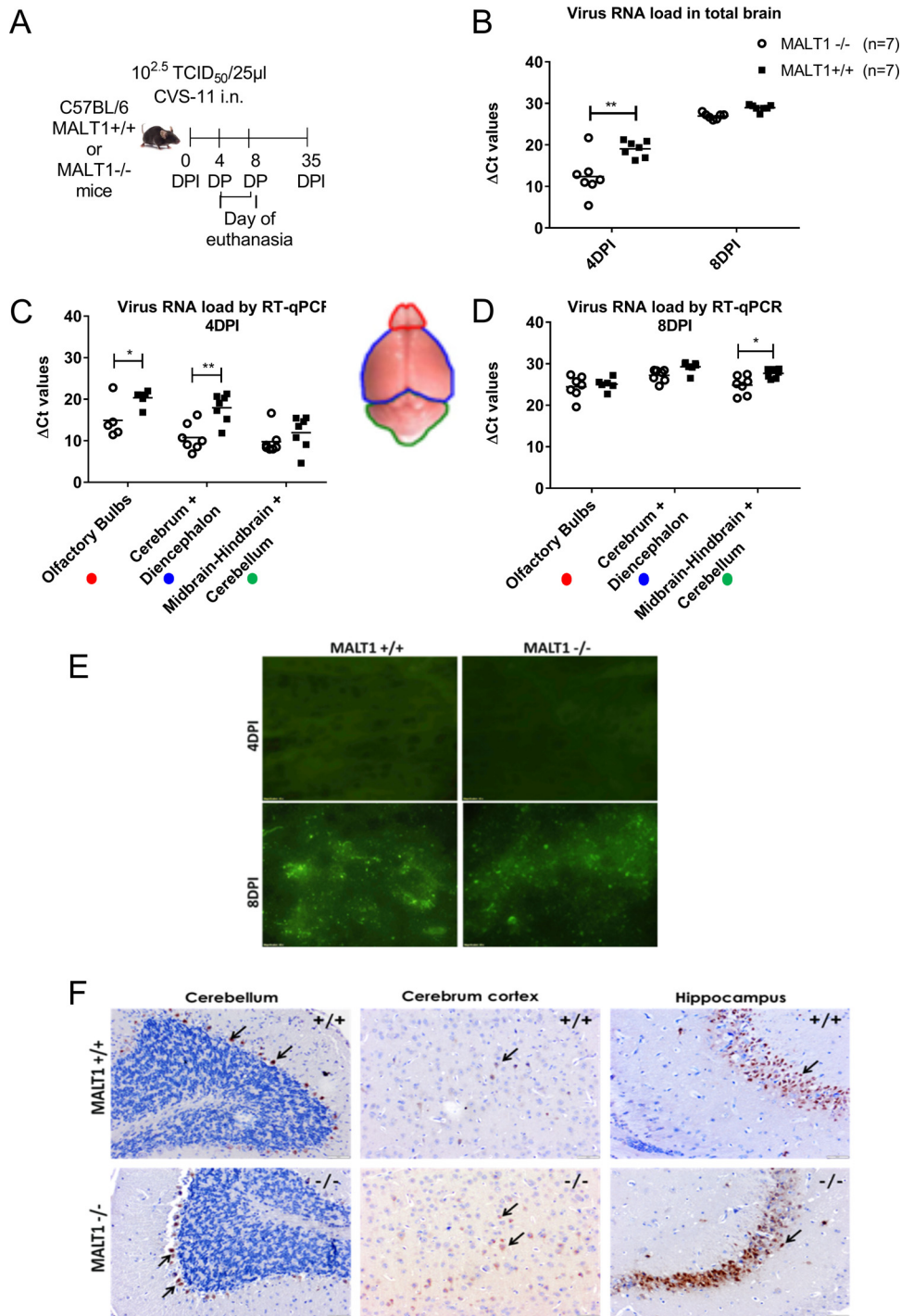
FIG 2 Virus spread in *Malt1*^{−/−} and *Malt1*^{+/+} mouse brain following intranasal inoculation of CVS-11 virus. (A) Schematic overview of the experiment. Mice were inoculated intranasally with the CVS-11 virus and sacrificed at 4 days postinoculation (dpi) and 8 dpi. (B) Profile of viral RNA in total brain in *Malt1*^{+/+} mice (*n* = 7) and *Malt1*^{−/−} mice (*n* = 7) at 4 and 8 dpi determined by RT-qPCR. C_T, threshold cycle. (C, D) Profile of viral RNA in different parts of the brain (*, *P* value ≤ 0.05; **, *P* value ≤ 0.01). (E) Immunofluorescence staining for viral nucleocapsid in the brain tissue. At 8 dpi, green fluorescent spots indicate the abundant spread of virus in the brain of *Malt1*^{−/−} and *Malt1*^{+/+} mice, but at 4 dpi no fluorescence could be detected yet. These results are representative of 3 mice per time point and per genotype. Bars, 20 μm; magnification, ×40. (E) Immunohistochemistry staining for viral G protein in the brain tissue. At 8 dpi, brown staining indicated by black arrows indicates the abundant spread of virus in the brain of *Malt1*^{−/−} and *Malt1*^{+/+} mice in the pyramidal cells of the hippocampus, Purkinje cells of the cerebellum, and cortical cells of the cerebrum. These results are representative of 2 mice per time point and per genotype. Bars, 20 μm (magnification, ×4) or 100 μm (magnification, ×10).
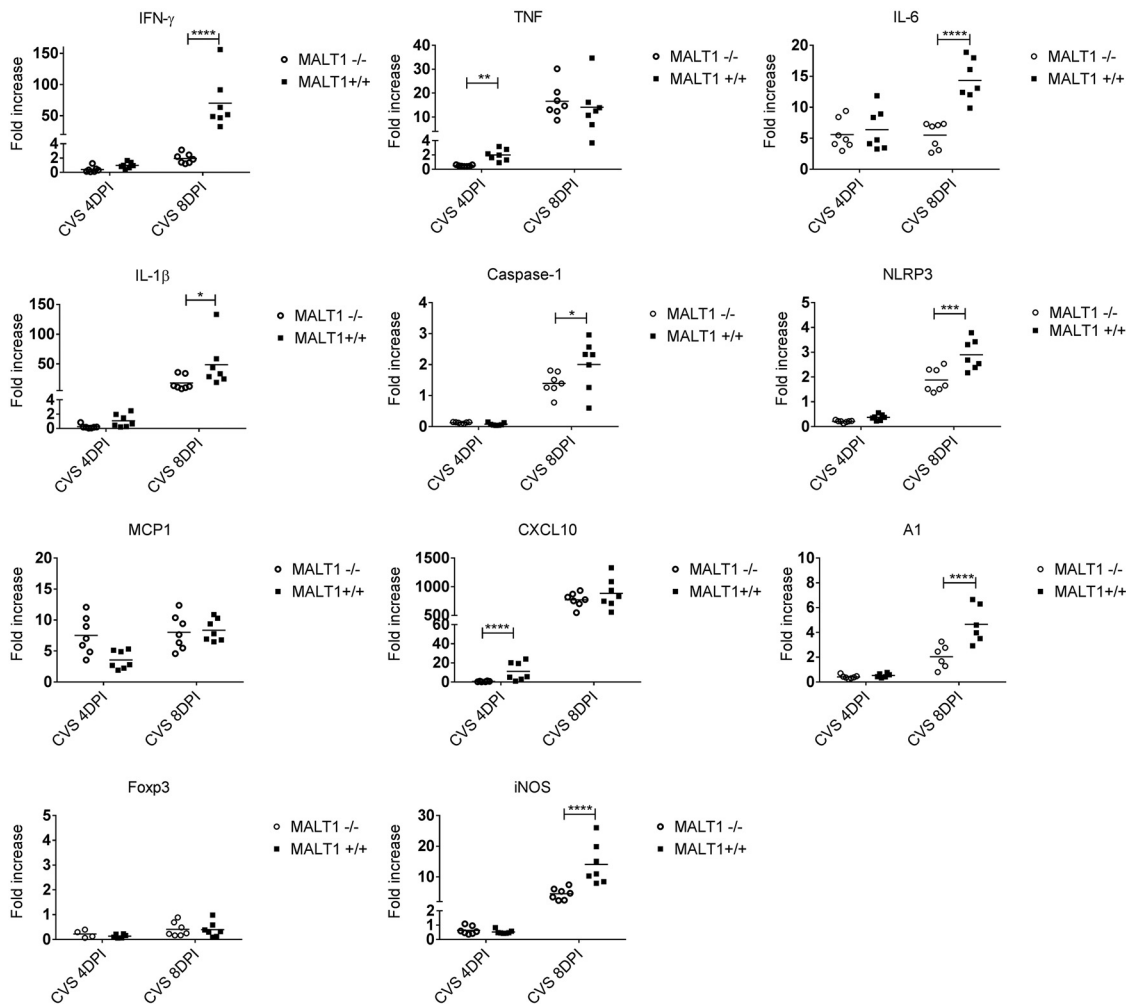
FIG 3 Decreased expression of inflammatory genes in the brain of infected MALT1$^{-/-}$ mice. Quantitative RT-qPCR measurements of the indicated mRNA expression levels in brains of *Malt1*$^{+/+}$ (n = 7) and *Malt1*$^{-/-}$ (n = 7) littermate mice are shown. Results are represented as fold increases compared to respectively noninfected *Malt1*$^{+/+}$ and *Malt1*$^{-/-}$ littermate mice. The asterisks indicate significant differences between infected *Malt1*$^{-/-}$ mice and CVS-11 virus-infected *Malt1*$^{+/+}$ mice at the same time points (4 dpi or 8 dpi) determined by two-way ANOVA and Sidak's multiple-comparison test. Statistical differences are denoted as follows: ****, $P < 0.0001$; ***, $P < 0.001$; **, $P < 0.01$; *, $P < 0.05$.

(PBS)-inoculated control mice. As expected, PBS-inoculated uninfected mice showed no activation of glial cells or enhanced brain immune surveillance (Fig. 4). *Malt1*$^{+/+}$ and *Malt1*$^{-/-}$ mice were infected intranasally with CVS-11, and brains were sampled at 4 and 8 dpi. At 4 dpi, stainings of *Malt1*$^{-/-}$ and *Malt1*$^{+/+}$ mouse brains were comparable to those of PBS-inoculated mice, suggesting that no detectable immune response was yet triggered in the CNS (data not shown). At 8 dpi, CVS-11-infected *Malt1*$^{+/+}$ mice exhibited strong microglial cell (Iba1 staining) and astrocyte (glial fibrillary acidic protein [GFAP] staining) activation and T or NKT cell (CD3 staining) and macrophage (Mac-3 staining) infiltration. However, no B cell (B220 staining) infiltration was detected. In comparison, CVS-11-infected MALT1$^{-/-}$ mice exhibited reduced microglial and astroglial cell activation, as well as reduced T, NKT cell, and macrophage infiltration. Again, no B cells were detected (Fig. 4).

Resting microglia were observed mainly in noninfected mice. They were characterized by their smaller cell body and long and ramified branch processes. Activated microglia were observed in both *Malt1*$^{-/-}$ and *Malt1*$^{+/+}$ brains at 8 dpi. Activation was evidenced by the typically bigger cell body and shorter and thicker branch processes but was strongly reduced in *Malt1*$^{-/-}$ brains. These differences were observed in different parts of the brain, including the hippocampus, cerebrum, and cerebellum (Fig. 5).
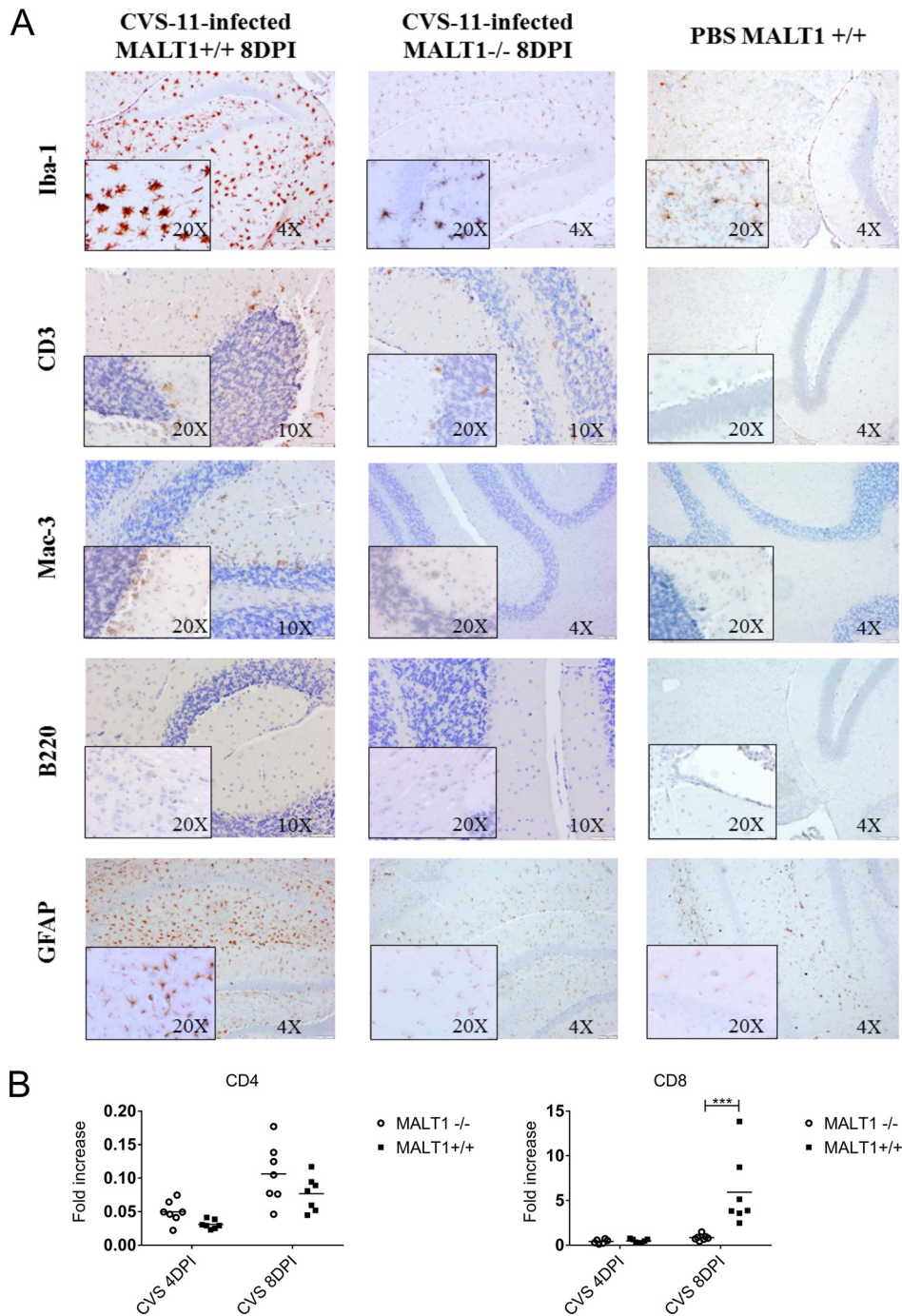
FIG 4 Reduced infiltration and activation of inflammatory cells in the brain of $Malt1^{-/-}$ mice at 8 dpi with CVS-11 virus. (A) Immunohistochemical analysis of CNS sections from infected $Malt1^{+/+}$ and $Malt1^{-/-}$ mice at 8 dpi. PBS-inoculated mice were used as controls. Sections of cerebellum and hippocampus are shown. Brain sections were immunostained for Iba1 (microglial cells), CD3 (T cells), Mac-3 (macrophages), B220 (B cells), and GFAP (astrocytes). PBS-injected $Malt1^{+/+}$ C57BL/6 mice showed abundant inactive ramified microglial cells and astrocytes, but no B cell, macrophage, or T cell infiltration. At 8 dpi, infected MALT1$^{+/+}$ mice showed activation of microglial and astroglial cells and infiltration of T lymphocytes and macrophages in the parenchyma but no B cell infiltration. In $Malt1^{-/-}$ mice, T lymphocyte and macrophage infiltration, as well as microglial/astrocyte activation, were reduced. Bars, 100 μm (magnification, ×4), 50 μm (magnification, ×10), or 20 μm (magnification, ×20). Data are representative of 2 mice per condition. (B) Quantitative RT-qPCR measurements of the indicated mRNA expression levels in brains of $Malt1^{+/+}$ ($n = 7$) and $Malt1^{-/-}$ ($n = 7$) littermate mice are shown. Results are represented as fold increases compared to respectively noninfected $Malt1^{+/+}$ and $Malt1^{-/-}$ littermate mice. The asterisks indicate significant differences between infected $Malt1^{-/-}$ mice and CVS virus-infected $Malt1^{+/+}$ mice at the same time points (4 dpi or 8 dpi) determined by two-way ANOVA and Sidak's multiple-comparison test. Statistical differences are denoted as follows: ****, $P < 0.0001$; ***, $P < 0.001$; **, $P < 0.01$; *, $P < 0.05$.
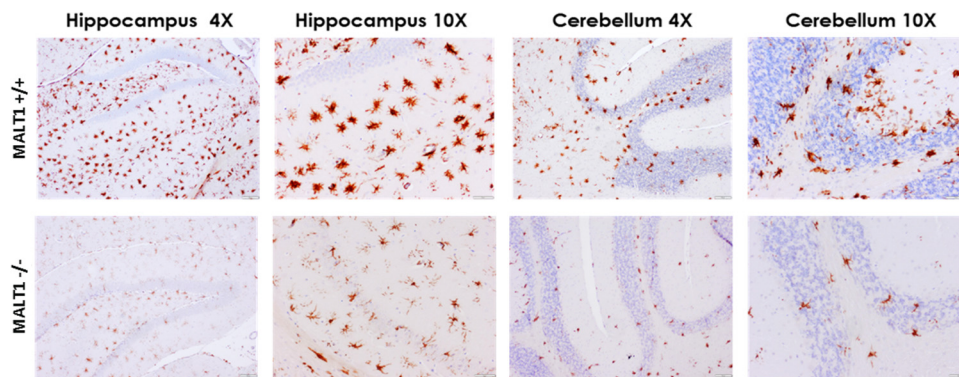
FIG 5 Reduced microglial activation at 8 dpi in the brains of *Malt1$^{-/-}$* mice. Immunohistochemical analysis of CNS sections from CVS-11-infected *Malt1$^{+/+}$* and *Malt1$^{-/-}$* mice at 8 dpi. Brain sections were immunostained for Iba1 (microglial cells). At 8 dpi, infected *Malt1$^{+/+}$* mice showed a strong microglial activation in the different parts of the brain (here, hippocampus and cerebellum). In *Malt1$^{-/-}$* mice, microglial activation was strongly reduced in all parts of the brain. Bars, 20 μm (magnification, ×4) or 100 μm (magnification, ×10). Data are representative of 2 mice per condition.

Inflammatory cell infiltration was also assessed by flow cytometric analysis of brain leukocytes at 8 dpi (Fig. 6A). CVS-11 infection in *Malt1$^{+/+}$* mice induced a high number of microglial cells (CD45$^{int/high}$ CD11b$^+$), and their activation was characterized by the switch from CD45^{int} CD11b$^+$ to CD45^{high} CD11b$^+$ and strong infiltration of monocytes/ macrophages/DCs (CD45^{high} CD11b$^+$), polymorphonuclear cells (Ly6G$^+$ CD11b$^+$), NK cells (CD49$^+$ CD3$^-$), NKT cells (CD49b$^+$ CD3$^+$), and T cells (CD49b$^-$ CD3$^+$) (Fig. 6B and C). In infected *Malt1$^{-/-}$* brains, the absolute number of total leukocytes was much lower than in infected *Malt1$^{+/+}$* brains (Fig. 6A). This is also reflected by lower numbers of CD3$^+$ T cells, NK cells, NKT cells, monocytes/macrophages/dendritic cells (DCs), microglial cells, and polymorphonuclear cells (Fig. 6C). Altogether, these data illustrate that MALT1 deficiency is associated with decreased infiltration and activation of inflammatory and immune cells in the brain upon CVS-11 virus infection.

To investigate if the humoral response was also affected by MALT1 deficiency upon CVS-11 infection, we measured the level of rabies virus-neutralizing antibodies in the serum. No neutralizing antibodies could be detected in the blood of either *Malt1$^{-/-}$* or *Malt1$^{+/+}$* mice upon infection with CVS-11. This suggests that the infection and the mortality are too fast for B cells to produce neutralizing antibodies. We were thus not able to show the involvement of MALT1 in B cell activation and antibody production due to the overall lack of an effective humoral response.

T-cell-specific MALT1 inactivation delays morbidity, but not as long as in complete knockout mice. MALT1 is ubiquitously expressed, and the delay in disease and mortality upon CVS-11 infection in *Malt1$^{-/-}$* mice may thus reflect a role for MALT1 in specific cell types belonging to lymphoid, myeloid, or neuronal lineages. We therefore generated conditional knockout mice lacking MALT1 in either T cells (CD4 Cre), myeloid cells (LysM Cre), cells of neuroectodermal origin (neurons, astrocytes, or oligodendrocytes; Nestin Cre), or NK cells (NKp46 iCre) and investigated their sensitivity to CVS-11 infection. T-cell-specific MALT1 knockout mice presented the first disease signs 1 day later than their wild-type littermates and also reached the endpoint of disease 1 to 2 days later. The delay in morbidity is less pronounced in T-cell-specific MALT1 knockout mice than in full MALT1 knockout mice (Fig. 7A to C), indicating a role for MALT1 expression in T cells as well as other cell types in viral pathogenesis. None of the other tested conditional MALT1-deficient mice showed a difference in terms of incubation period, clinical signs, and mortality compared to their wild-type littermates (Fig. 7B, D, and E), indicating that the phenotype observed in MALT1 full-knockout mice is not linked to the absence of MALT1 in natural killer cells, myeloid cells, neurons, astrocytes, or oligodendrocytes.

Inhibition of MALT1 proteolytic activity decreases morbidity in infected mice. *Malt1$^{-/-}$* mice do not allow us to draw any conclusions on the relative role of its
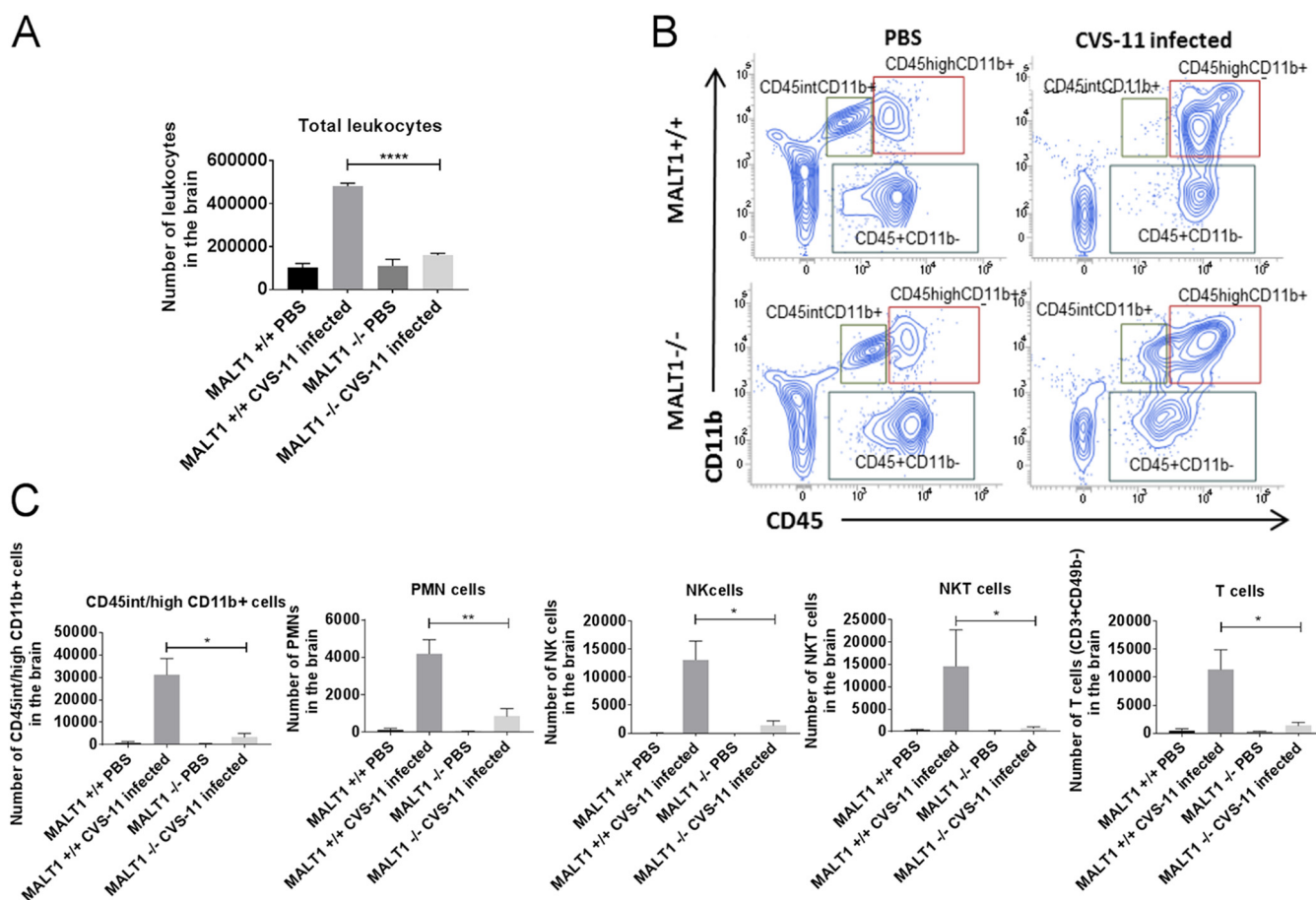
FIG 6 Flow cytometric analysis of inflammatory and immune cell activation and infiltration in the brain of infected mice. Immune cells were isolated from the brains of naive mice and infected mice (*Malt1*^{+/+} and *Malt1*^{−/−}) at 8 dpi. (A) Absolute numbers of leukocytes present in the brain were first determined, and total numbers of each cell type were determined by the percentage of marker expression on the total number of leukocytes. A significant decrease of total leukocytes was observed in infected *Malt1*^{−/−} mice compared to infected *Malt1*^{+/+} mice. (B) CD45 and CD11b markers were used to distinguish T cells (CD3^{+} CD11b^{−} CD45^{high}), microglial cells (CD11b^{+} CD45[int/high]), and monocytes/macrophages/DCs (CD11b^{+} CD45^{high}). (C) Gate was placed on CD45^{+} CD11b^{−} cells, and CD49b and CD3 markers were also used to distinguish NK cells (CD49b^{+} CD3^{−}), NKT cells (CD49b^{+} CD3^{+}), and T cells (CD49b^{−} CD3^{+}). Gate was also placed on CD45^{+} CD11b^{+}, and an Ly6G marker was used to distinguish PMN cells. A significant decrease of microglial cells/monocytes/macrophages/DCs, Ly6G^{+} PMN cells, NK cells, NKT cells, and CD3^{+} CD49^{−} T cells was observed in infected *Malt1*^{−/−} mice compared to infected *Malt1*^{+/+} mice. Dot plots are representative results for at least 3 mice per condition. Statistical differences between *Malt1*^{+/+} and *Malt1*^{−/−} mice were determined using Student's *t* test and are denoted as follows: ***, $P < 0.001$; **, $P < 0.01$; *, $P < 0.05$. Data are representative of two independent experiments.

scaffold and proteolytic activities, respectively. To investigate the specific role of MALT1 catalytic activity in the pathogenicity of CVS-11 virus, we first analyzed the effect of pharmacological inhibition of MALT1 catalytic activity using the phenothiazine mepazine, which was previously shown to act as a reversible MALT1 inhibitor (40). Mice were treated twice a day intranasally with mepazine or 0.9% NaCl (control), starting 2 days before CVS-11 inoculation (Fig. 8A). Mice treated with PBS reached the endpoint of disease at 8 days after inoculation with CVS-11, whereas in mice treated with mepazine this occurred about 2 days later (median survival time, 10 days; Fig. 8B). These data indicate an important role for MALT1 catalytic activity in the pathogenicity of CVS-11 rabies virus infection.

Because the specificity of mepazine as a MALT1 inhibitor has recently been questioned (41), we also took advantage of a genetic approach to study the effect of specific inhibition of MALT1 proteolytic activity. Therefore, MALT1[PD/−] knock-in mice (expressing one mutant protease-dead MALT1 allele and lacking MALT1 on the other allele) were infected with CVS-11 and analyzed for disease symptoms. Similar to the effect of mepazine, disease development was significantly delayed in *Malt1*[PD/−] mice compared to *Malt1*^{+/−} littermate control mice (Fig. 8C). It should be mentioned that the protec-
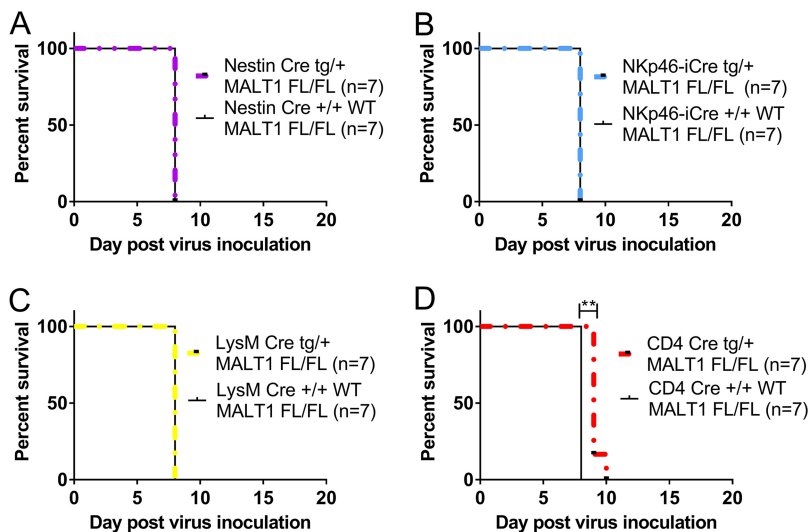
FIG 7 Impact of specific inactivation of MALT1 in T cells, myeloid cells, NK cells, and cells from neuroectodermal origin on CVS-11 virus infection. Mice with the CRE recombinase under the influence of the CD4, LysM, NKp46, or Nestin promoter were crossed with MALT1$^{FL/FL}$ mice to generate conditional mice lacking MALT1 in T cells, myeloid cells, NK cells, or cells from neuroectodermal origin, respectively. Conditional mice and their wild-type littermates were genotyped and selected for each experiment. Mice were infected intranasally with CVS-11 virus and monitored for disease development and survival. Mice lacking MALT1 in cells from neuroectodermal origin (Nestin-Cre$^{tg/+}$ $Malt1^{FL/FL}$) (A), NK cells (NKp46-iCre$^{tg/+}$ $Malt1^{FL/FL}$) (B), and myeloid cells (LysM-Cre$^{tg/+}$ $Malt1^{FL/FL}$) (C) developed the same evolution of disease as their wild-type littermates. (D) Mice lacking MALT1 in T cells (CD4$^-$ Cre$^{tg/+}$ $Malt1^{FL/FL}$) presented the first symptoms later than their wild-type littermates and had to be sacrificed 1 to 2 days later, which is, however, still earlier than in full $Malt1^{-/-}$ mice.

tive effect is less pronounced than the effect seen after complete inhibition of MALT1 in all cell types, suggesting that both the scaffold and catalytic activities of MALT1 contribute to virus pathogenicity. Importantly, these data also illustrate the possible use of MALT1 inhibitors for therapeutic intervention in rabies infection.
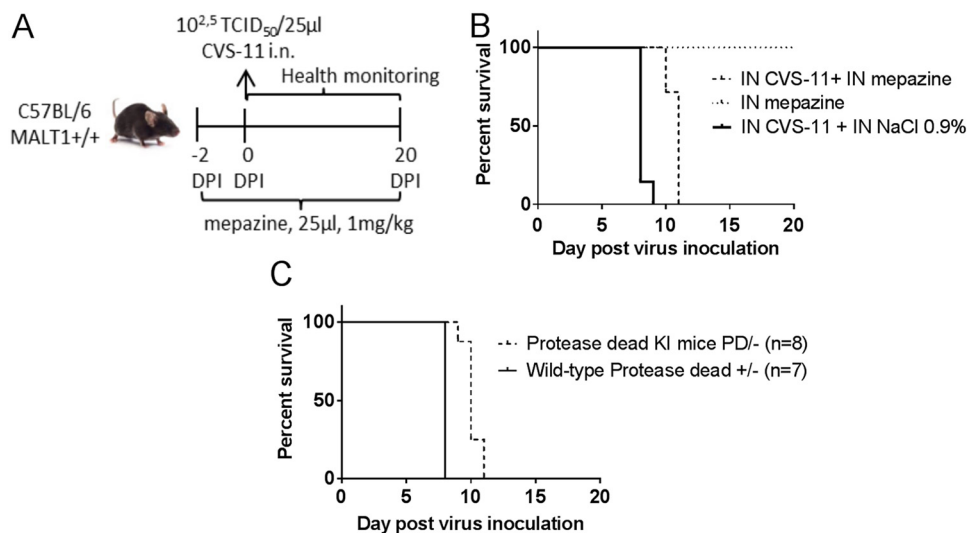
FIG 8 Impact of pharmacological or genetic inhibition of MALT1 catalytic activity on survival of CVS-11-infected mice. (A) Schematic overview of the pharmacological approach. Wild-type mice were treated twice a day with mepazine ($n = 7$) or a control solution (0.9% NaCl in water) ($n = 7$) starting at day -2 before virus inoculation until the end of the experiment. Two days after the first treatment, mice were inoculated intranasally with CVS-11 virus and monitored daily for signs of disease. (B) Survival curves of mepazine-treated mice infected with CVS. (C) Survival curves of protease-dead MALT1 knock-in mice infected with CVS.

DISCUSSION

Rabies virus is a neurotropic virus inducing acute and lethal infection in the CNS. The exact mechanisms causing death are not yet fully understood. Some studies proposed that death is related to neuronal exhaustion and hormonal deregulation (42–44), but it cannot be excluded that other factors are involved. In this context, the proinflammatory neuronal environment may also contribute to lethality (45–47).

In the present study, we show that infection of C57BL/6 mice with a highly virulent rabies virus results in rapid disease development, requiring euthanasia at 8 dpi. Illness was accompanied by an early increase of CXCL10, CD8, iNOS, TNF, IFN-γ, IL-6, IL-1β, A1 mRNA levels, microglial/astroglial activation, and infiltration of T cells/macrophages/DCs/polymorphonuclear leukocytes (PMNs)/NK(T) cells in the brain. In $Malt1^{-/-}$ mice, the development of clinical signs and mortality were significantly delayed compared to what was seen in littermate $Malt1^{+/+}$ mice. Deficiency of MALT1 also led to lower viral loads in the beginning of infection (4 dpi) and less neuroinflammation at the later stage (8 dpi), which was associated with reduced cytokine, chemokine, and iNOS expression, less infiltration of CD8$^+$ T cells, myeloid cells, and NK(T) cells, and less activation of microglial and astroglial cells. The prolonged incubation period in $Malt1^{-/-}$ mice may thus be explained by lower viral loads and/or reduced neuroinflammation. We speculate that lower viral loads in the beginning of infection reflect a role for MALT1-dependent cellular processes that facilitate virus replication and/or spread. However, disease development was not delayed in mice lacking MALT1 exclusively in cells from neuroectodermal origin, which are the primary target cells of the virus. Therefore, the reduced neuroinflammation in $Malt1^{-/-}$ mice most likely has a major impact on disease progression. In this context, MALT1-mediated neuroinflammation was already shown to play an important role in a murine model of multiple sclerosis, with $Malt1^{-/-}$ mice failing to recruit myeloid cells in the CNS and proinflammatory and Th17 responses being severely impaired (34, 48).

Using cell type-specific MALT1 knockout mice, we show that specific inactivation of MALT1 in T cells also delays CVS-11 rabies virus-induced clinical symptoms and mortality, although the effect is less pronounced than the protection seen in complete $Malt1^{-/-}$ mice (1 to 2 days versus 4 days). These data indicate a role for MALT1 signaling in T cells, but also other cell types, in MALT1-mediated neuroinflammation and pathogenesis in response to CVS-11 rabies virus infection. T-cell infiltration can be beneficial for viral clearance in the brain, but an excess of T cells can also be deleterious because it causes greater inflammation-induced damage. The pathogenic role of T cells in rabies virus infection has previously been investigated in a number of studies. Mice infected with a street isolate of rabies virus present strong T-cell infiltration in the dorsal root ganglia and elevated levels of mRNA transcripts of IFN-α/β, IFN-γ, CCL5, and CXCL10 in the brain, and it was suggested that damage to the dorsal root ganglia may be due to a combination of virus infection and T-cell infiltration (49). Other studies showed that T cells can enter the brain but then undergo virus-induced apoptosis (11, 50, 51). Overall, the contribution of T cells in clearing virulent rabies virus from the brain is believed to be rather limited, which is consistent with our finding that T-cell-specific MALT1 deletion has only an intermediate effect on CVS-11 mortality compared to deletion in all cells. In contrast, T cells are much more important in controlling infections caused by attenuated viruses, in which T cells remain intact and infected neurons can be eliminated (52, 53). This is also supported by our recent finding that MALT1 deficiency in T cells, leading to decreased T cell activation, strongly sensitizes mice to infection with the attenuated rabies virus strain ERA (54).

In our experiments, we could not detect virus-neutralizing antibodies in the serum of infected mice before they died. Considering the lack of a humoral immune response as well as the limited role of T cells, it is therefore likely that MALT1-mediated innate immune responses also contribute to the pathogenicity. A similar role of innate immunity to morbidity during neurotropic viral infections was already observed for West Nile virus infection (55). Moreover, a deleterious involvement of an innate immune

response following infection with another virulent rabies virus strain (CVS-NIV) was suggested before. More specifically, Chopy et al. showed that transgenic mice overexpressing LGP2, an enigmatic member of the RIG-I like receptor family that senses viral RNA, exhibit a drastic reduction in rabies virus-induced innate immune responses and low morbidity compared to wild-type mice, revealing a pathogenic role of the RIG-I-mediated innate immune response in rabies virus infection (9). Of interest, RIG-I-induced NF-κB activation and cytokine production in vesicular stomatitis virus (VSV)-stimulated dendritic cells are strongly reduced in CARD9- and BCL10-deficient cells, while interferon responses are normal (56). Remarkably, in the latter study, MALT1 was entirely dispensable for RIG-I-induced NF-κB activation, but its role in RIG-I-mediated IFN regulatory factor 3 (IRF3) activation and type I interferon production remains to be determined. In this context, CARD10, another protein known to be engaged in a signaling module with BCL10 and MALT1, was also shown to positively regulate RIG-I-mediated activation of NF-κB and proinflammatory cytokine expression in mouse embryonic fibroblasts and lung epithelial cells but to negatively regulate RIG-I-mediated activation of IRF3 and type I IFN expression by suppressing oligomerization of the adaptor protein MAVS (57). In agreement, CARD10-deficient mice had a lower viral load and higher production of type I IFN 1 day after intranasal infection with VSV. The decreased viral load that we observed in our present study with rabies-infected $Malt1^{-/-}$ mice makes it tempting to speculate a similar negative regulatory role for MALT1 and specific CARD family members in RIG-I-induced IRF3 signaling in rabies-infected cells.

The specific cell type, besides T cells, in which MALT1-mediated signaling contributes to CVS-11 virus-induced pathogenesis remains to be identified. Using several conditional MALT1 knockout mice, we can already exclude a role for MALT1 expression in myeloid cells, NK cells, or neuronal cells. It is important to mention, however, that the LysM promoter used to generate conditional mice lacking MALT1 in myeloid cells is almost not present in microglial cells (58). Within the CNS, microglial cells are tissue macrophages with a neuroprotective role that act as scavenger cells by phagocytosing dead cells. However, microglial cells can also be detrimental for the CNS by releasing cytokines and inflammatory molecules such as IL-1β, TNF, and nitric oxide, leading to neuronal death. Microglial and astroglial cells were previously shown to be activated following CVS-11 infection in mice (59). Here we show that both microglial and astroglial cells are activated in all parts of the brain at 8 dpi, which is associated with a change in morphology from ramified (inactive) to amoeboid (activated). Considering the important difference of microglial activation between $Malt1^{-/-}$ and $Malt1^{+/+}$ mice, it is possible that MALT1 activation in microglial cells is a key immunopathologic event during rabies virus infection. Similarly, activation of microglial cells has already been shown to contribute to the pathogenesis of a variety of neurodegenerative diseases, such as Alzheimer disease, Parkinson disease, and AIDS dementia complex (60–63). It will therefore be of interest to analyze in the future the effect of CVS-11 infection in mice in which MALT1 is specifically deleted in microglial cells. Unfortunately, a Cre mouse line that specifically deletes MALT1 in microglial cells is not yet available. CX3CR1 cre-ERT mice are known to delete XXX in microglial cells (64), but CX3CR1 is also expressed in macrophages, NK cells, and circulating T and B cells, limiting the usefulness of these mice.

Several cytokines (e.g., TNF, IL-6) or other mediators (e.g., NO) released by microglial cells, but also other cell types, may contribute to virus-induced neurotoxicity (65, 66). In our present study, rabies virus-induced expression of many cytokines, including TNF, IL-1β, and IL-6, was reduced in $Malt1^{-/-}$ mice. Camelo et al. showed that TNF receptor 1 deficiency extends survival of CVS-11 infected mice, suggesting a deleterious effect of TNF signaling (67). In this context, TNF was also suggested to induce weight loss, paralysis, and wasting syndrome in CVS-11 infection. TNF may cause neurotoxicity either directly by triggering neuron apoptosis or indirectly by inducing neuronal dysfunction due to the activation of microglia (44). Recently, treatment of mice with a TNF inhibitor (infliximab), but also an IL-6 inhibitor (tocilizumab), was shown to extend

the survival time of rabies-infected mice (68). Previously, we found that IL-1β did not contribute to the morbidity upon CVS-11 infection (69). Several studies indicated that NO production in the brain during rabies virus infection correlates with neuropathology, suggesting that increased iNOS activity leads to tissue damage in the CNS and more-severe clinical signs (70–73). In agreement, the iNOS inhibitor aminoguanidine was shown to decrease NO production and TNF expression and to delay the development of clinical signs upon CVS-11 infection in mice (71). It has also been reported that NO is toxic to neurons, causing neuronal dysfunction (74). Together, these findings suggest that the marked increase in iNOS levels in rabies virus-infected mice contributes to the pathogenesis by promoting inflammation and apoptosis. Considering the strong activation of microglia and infiltration of macrophages in the brain of CVS-11-infected mice, increased iNOS expression and NO production by macrophages and microglial cells likely play an important pathological role, and reduced iNOS expression, together with reduced TNF and IL-6 expression, may be responsible for the lower morbidity in $Malt1^{-/-}$ mice.

Importantly, pharmacological as well as genetic inhibition of MALT1 proteolytic activity also delayed disease onset and extended survival in CVS-11-infected mice, illustrating a key role for MALT1 catalytic activity in the pathogenic response. Moreover, these results illustrate the potential of therapeutic targeting of MALT1 in the context of lethal rabies infection. To date, several MALT1 inhibitors have been described, and many others are currently in development for the treatment of autoimmunity and certain types of cancer (41). The fact that MALT1 inhibition only slows down rabies-induced disease progression and cannot prevent lethality may jeopardize such an approach, but extended survival upon initial treatment with MALT1 inhibitors may allow more time for postexposure prophylaxis or other treatments to be effective in acute encephalitis caused by highly virulent rabies viruses. The here-described protective effect of MALT1 inhibition in mice infected with the virulent rabies virus strain CVS-11 is in sharp contrast to the sensitizing effect of MALT1 inhibition that we previously reported in mice infected with an attenuated vaccine rabies virus strain (ERA), which was shown to result from decreased MALT1-mediated T cell activation in the early phase of infection (54). Experimental work with attenuated rabies viruses can give insights on how rabies virus can be controlled and cleared from the brain by the immune system, whereas the use of virulent rabies viruses allows to study the mechanisms of acute and lethal rabies disease. In this context, we showed that MALT1 was required for the effective clearance of virus strain ERA, which is less pathogenic than the rabies virus strain CVS-11. On the other hand, in this study, we showed that MALT1 contributes to the acute immunopathology caused by the virulent strain CVS-11. In the case of a virulent rabies strain, the MALT1-driven immune system fails to clear the virus and rather contributes to disease. Together, these studies provide novel insights in the biology of MALT1 and rabies virus infection, demonstrating that the effect of an inflammatory response on the outcome of rabies virus infection may differ depending on the virulence of the virus. However, it should be mentioned that CVS-11 is a mouse-adapted rabies virus strain and cannot be considered a prototype rabies street strain because of its long-term adaptation to mice. For future purposes, it would also be valuable to analyze infection of $Malt1^{-/-}$ mice with a street rabies virus strain. Future studies should also focus on the elucidation of the underlying molecular mechanisms that lead to MALT1 signaling and the specific cell types involved. Moreover, it will be of interest to study if MALT1 plays a similar role in cases of infection with other encephalitic viruses.

MATERIALS AND METHODS

Mice. $Malt1^{-/-}$ mice were generously provided by the team of Tak Mak (32). Mice were backcrossed for more than 10 generations into the C57BL/6 background and were intercrossed to generate $Malt1^{+/+}$, $Malt1^{+/-}$, and $Malt1^{-/-}$ offspring. Cell type- or lineage-specific $Malt1$-deficient mice were obtained as described previously (54), and NKp46-iCre line mice (75) were kindly given by Eric Vivier. MALT1 PD mice lacking only the catalytic activity of MALT1 were generated by crossing $Malt1^{-/-}$ and $Malt1^{PD/+}$ mice (provided by M. Baens). All mice were bred and housed in filtered cages in temperature-controlled,

air-conditioned facilities with 14/10-h light/dark cycles and food and water *ad libitum* and were used at the age of 6 to 12 weeks. All experimental procedures were approved by the Local Ethical Committee of the Scientific Institute of Public Health (WIV-ISP) and the Veterinary and Agrochemical Research Center (CODA-CERVA).

Genotyping. $Malt1^{-/-}$, $Malt1^{+/+}$, and $Malt1^{+/-}$ mice and conditional mice were genotyped as described in reference 54. For NKp46iCre mice, the NKp46iCre KI transgene was detected with the primers 2636 (CAC TCC TAC CCC TTC ATT TCT GA), 2638 (ACC GCC TGA TCT ATG GTG CC), and 2640 (GGG TGG GTG TAG CCT CTA TC), which results in 352-bp (+) or 257-bp (KI) PCR fragments. $Malt1$ protease-dead ($Malt1$ PD mice) were genotyped using the primers F-MALT-KICA-GT (CCCACTCCCAGGATTGTTAT ATT), R-MALT1-KICA-GT (TGC TCT AGA TCC ACA GGT GTG GTT), KI-MALT-CA-F (AAT GTG TTC CTG TTG GAT ATG GCC AG), and KI-MALT-WT-R (GAG ACA TTT TAC CTT TTC CGA CAC), which resulted in PCR fragments of 461 bp (allele independent), 304 bp (PD), or 201 bp (wild type). Transgenic mice were identified by PCR analysis of genomic DNA extracted from tails and amplification of the selected fragments using the GoTaq G2 DNA polymerase (Promega, Madison, WI, USA) master mix, with a typical PCR program: 5 min of 95°C denaturation, 35 to 40 cycles of 30 s at 95°C, 30 s at 55 to 60°C, and 60 s at 72°C, and 10 min at 72°C for final elongation. Fragments were visualized on a 2% agarose gel.

Virus. The highly virulent neurotropic challenge virus standard 11 (CVS-11) strain was obtained from the American Type Culture Collection (ATCC; reference number VR959). Viral stocks were produced in baby hamster kidney 21 (BHK-21) cells (Deutsche Sammlung von Mikroorganismen und Zellkulturen GmbH, Braunschweig, Germany). The lysates of infected cell cultures were centrifuged at $20,000 \times g$ for 20 min at 4°C, and supernatants were stored at −80°C.

Virus titration. Infectious rabies virus particles were titrated by endpoint dilution assay in BHK-21 cells. Results were expressed as 50% tissue culture infective doses ($TCID_{50}$) per milliliter, which represents the amount of virus per milliliter that gives rise to infection in 50% of inoculated tissue culture cells. Virus titration was performed according to the *Manual of Diagnostic Tests and Vaccines for Terrestrial Animals* from the Office International des Epizooties (76).

Viral infection, clinical follow-up, euthanasia, and sampling. Mice were inoculated intranasally with CVS-11 using $10^{2.5}$ 50% $TCID_{50}$ in 25 μl of PBS during brief anesthesia with isoflurane as described by Rosseels et al. (19). Mice were observed once a day for signs of disease throughout the experiment until 35 days dpi. A cumulative daily clinical score per mouse was obtained by adding the scores for each parameter. A score ranging from 0 (no disease) to 9 (severe brain disease) was attributed to each mouse. Disease signs were scored as described previously (54). Once the mice reached a minimum score of 6 or at different time points following virus inoculation (4 dpi is the incubation phase, and 8 dpi is the end stage of disease), they were euthanized with an overdose of ketamine (100 mg/kg of body weight; Ceva, Brussels, Belgium) and xylazine (9.9 mg/kg; Rompun 2%; Bayer Healthcare, Kiel, Germany) given intra-peritoneally (i.p.) at a dose of 300 μl/mouse. The blood was flushed from the circulatory system by transcardial perfusion with a PBS solution. Brains were collected and were divided in two halves according to a longitudinal section. One half was stored at −80°C for further analysis by real-time quantitative reverse transcriptase PCR (RT-qPCR) or fluorescent antigen test (FAT), and the other half was submerged in 4% formaldehyde for fixation. Paraffin-embedded sections of 2-μm thickness were made for further immunohistochemical analysis. Serum was collected from mice at different time points postinoculation and upon euthanasia for titration of virus-neutralizing antibodies. Mice that did not develop disease signs were anesthetized, perfused, and euthanized at 35 dpi.

Treatment with mepazine. Mepazine hydrochloride (Merck Millipore) was solubilized in physiolog-ical water (0.9% NaCl) at a concentration of 2 mg/ml. Mice were treated intranasally twice daily (1 mg/kg) with 25 μl of either mepazine or 0.9% NaCl starting 2 days before virus inoculation (with CVS-11) and until the end of the experiment.

RNA extraction and real-time quantitative reverse transcriptase PCR assay for quantification of the CVS-11 virus and immune and inflammatory gene expression. Seven mice per group were euthanized at each indicated time point. RNA extraction was performed using the RNeasy minikit (Qiagen, Hilden, Germany) according to the manufacturer's instructions. RNA concentration was calcu-lated using Nano Vue spectrophotometry (GE Healthcare, Bucks, UK), and 100 ng was engaged in reverse transcription. Reverse transcription and quantitative PCR (qPCR) were performed as described by Rosseels et al. (19). Two primers located in the nucleoprotein N genome region were used for the detection of CVS-11 virus, and other primer sequences were used for the amplification of immune genes (all primer sequences are accessible on demand). All samples were analyzed in duplicate. Amplification was performed on an iCycler iQ from Bio-Rad in a 96-well optical plate format, using the following program: 2 min at 95°C followed by 45 cycles of 20 s at 95°C and 30 s at 62°C. A melting curve analysis was performed in order to verify the specificity of amplicons. Expression of all genes was normalized using the cellular 18S rRNA housekeeping gene. Quantification of viral N gene and immune gene expression was performed as described in reference 54.

Titration of neutralizing antibody in the blood by RFFIT. Mouse blood samples were used for measurement of neutralizing antibodies using the rapid fluorescent focus inhibition test (RFFIT) accord-ing to the *Manual of Diagnostic Tests and Vaccines for Terrestrial Animals* (76). Neutralizing antibody titers are expressed as international units per milliliter using as a reference "The second international standard for anti-rabies immunoglobulin," purchased from the United Kingdom National Institute for Biological Standards and Control. Serum titer levels of 0.5 IU/ml or higher are an indication of seroconversion.

Detection of nucleocapsid antigen of rabies virus by FAT and glycoprotein antigen of rabies virus by IHC. FAT was performed according to the *Manual of Diagnostic Tests and Vaccines for Terrestrial Animals* (76). Brain smears were fixed with 75% acetone for 30 min at −20°C and incubated with

fluorescein isothiocyanate (FITC)-coupled antinucleocapsid rabbit antibody (Bio-Rad, Marne-la-Coquette, France) for 30 min at 37°C. Positive signals were visualized under the fluorescence microscope.

For IHC, virus-inoculated mice and PBS-inoculated mice were transcardially perfused with PBS. Brains were removed, immersed in 4% paraformaldehyde, dehydrated, and embedded in paraffin blocks. Sections of 2 μm were made and were deparaffinized and rehydrated in descending grades of ethanol and then distilled water. Sections were then microwaved in 10 mM trisodium citrate buffer (pH 6.0; Dako-Agilent Technologies, Santa Clara, CA, USA) for antigen retrieval. Nonspecific antigen binding sites were blocked with 5% normal goat serum (Dako-Agilent Technologies, Santa Clara, CA, USA). To remove endogenous peroxidase, sections were treated with peroxidase block (kit Dako Envision; Dako-Agilent Technologies, Santa Clara, CA, USA) for 5 min. After washing, sections were incubated with primary monoclonal mouse anti-rabies antibody (Anti-Rabies, catalog number 3R7 MAb 1C5; HyTest Ltd., Finland) for 30 min, diluted at 1/100 in Dako antibody diluent with background reducing components (Dako-Agilent Technologies, Santa Clara, CA, USA). Sections were washed in 1× Dako wash buffer (Dako-Agilent Technologies, Santa Clara, CA, USA), and one droplet of labeled polymer-horseradish peroxidase (HRP) anti-mouse antibody (kit Dako Envision; Dako-Agilent Technologies, Santa Clara, CA, USA) was added to each section for 30 min. After washing, sections were incubated with 3.3′-diaminobenzidine (DAB) chromogen (kit Dako Envision; Dako-Agilent Technologies, Santa Clara, CA, USA) until the desired staining developed and then were counterstained with Meyer's hematoxylin and eosin (Dako-Agilent Technologies, Santa Clara, CA, USA), dehydrated, and mounted in a xylene-based mounting medium (Entellan; Merck Life Science, Darmstadt, Germany). Stainings were visualized under the light microscope.

Immunohistological analysis of mouse brains for expression of Iba1, GFAP, B220, CD3, and Mac-3. For detection of immune cells by IHC, brain sections were deparaffinized and rehydrated in descending grades of ethanol and then distilled water. Microglial cell, astrocytes, B cells, T cells, and macrophages were detected using specific antibodies: rabbit anti-Iba1 (Wako Chemicals, Fuggerstraβe, Germany), rabbit anti-GFAP (Dako-Agilent Technologies, Santa Clara, CA, USA), rat anti-B220 (eBioscience-Thermo Fisher Scientific, Waltham, MA, USA), rabbit anti-CD3 (Dako-Agilent Technologies, Santa Clara, CA, USA), and rat anti-Mac-3 (BD Pharmingen, San Diego, CA, USA), respectively. Sections were incubated in 10 mM citrate buffer (Dako-Agilent Technologies, Santa Clara, CA, USA) for 10 min at 95°C. To remove endogenous peroxidase, sections were treated with 3% H_2O_2 in methanol. To block nonspecific reactions, each section was treated with 5% goat serum in antibody diluent (Dako-Agilent Technologies, Santa Clara, CA, USA) for 30 min. Primary antibody was diluted in 5% goat serum in antibody diluent with the dilution depending on the staining performed (Iba1, 1/1,000; CD3, 1/200; MAC-3, 1/250; B220, 1/1,000; GFAP, 1/200,000) and incubated on brain sections overnight at 4°C. Goat anti-rabbit (Dako-Agilent Technologies, Santa Clara, CA, USA) or goat anti-rat (BD Pharmingen, San Diego, CA, USA) secondary antibodies conjugated to biotin were diluted at 1:500 in block buffer and added for 45 min to 1 h to the sections. Drops of avidin/biotin-based peroxidase system Vectastrain Elite ABC (Vector laboratories, Burlingame, CA, USA) were added to each section for 30 min. Finally, antibody was visualized using DAB (Dako-Agilent Technologies, Santa Clara, CA, USA) until specific staining appeared. Slides were counter-stained with hematoxylin, dehydrated, and mounted with a xylene-based mounting medium (Entellan; Merck Life Science, Darmstadt, Germany). Sections without primary antibody were taken also, as controls. Stainings were visualized under a light microscope.

Immunophenotyping of leukocytes in the brain. Immune cells were extracted from the brain at 8 dpi as described previously (77). In brief, brains were collected, and single-cell suspensions were prepared by gently pressing the organs in Hanks balanced salt solution (HBSS) through a nylon mesh (mesh size, 100 μm). After centrifugation, cells were placed in collagenase-DNase for 1 h. After washing, the suspension was centrifuged in 25% Percoll (Sigma-Aldrich, St. Louis, MO, USA), the myelin layer was removed, and cells were suspended in HBSS containing 10% fetal calf serum (FCS). Red blood cell lysis buffer was added to the cell pellet to eliminate erythrocytes. Cells were washed twice with fluorescence-activated cell sorter (FACS) buffer (PBS containing 10% FCS and 0.1% NaN$_3$) and incubated with FcγII/III receptor blocking anti-CD16/CD32 (clone 2.4G2; BD Biosciences, San Jose, CA, USA) for 15 min at 4°C. Cells were then incubated for 30 min at 4°C protected from light with viability dye (Thermo Fisher) and the appropriate dilutions of the following antibodies: APC-e780-anti-CD45 (clone 30F11), FITC-anti Ly6G (clone 148), e450 anti-CD11b (clone M1/70), PE-anti-CD49b (clone DX5), PerCP-anti-CD3 (clone 145-2C11). The stained cells were washed twice in FACS buffer, fixed with 4% paraformaldehyde, and analyzed in a BD FACSVerse flow cytometer. Data were analyzed using BD FACSuite software. Antibodies were from BD Pharmingen or Thermo Fisher.

Statistical analyses. Statistical analysis was performed using the Student t test for unpaired data or the 2-way analysis of variance (ANOVA) followed by a Sidak multiple-comparison test in GraphPad Prism7. The log rank test was used to analyze Kaplan-Meier survival curves.

REFERENCES

1. Jackson AC. 2008. Rabies. Neurol Clin 26:717–726, ix. https://doi.org/10.1016/j.ncl.2008.03.010.
2. Hampson K, Dushoff J, Cleaveland S, Haydon DT, Kaare M, Packer C, Dobson A. 2009. Transmission dynamics and prospects for the elimination of canine rabies. PLoS Biol 7:e53. https://doi.org/10.1371/journal.pbio.1000053.
3. Hampson K, Coudeville L, Lembo T, Sambo M, Kieffer A, Attlan M, Barrat J, Blanton JD, Briggs DJ, Cleaveland S, Costa P, Freuling CM, Hiby E, Knopf L, Leanes F, Meslin F-X, Metlin A, Miranda ME, Muller T, Nel LH, Recuenco S, Rupprecht CE, Schumacher C, Taylor L, Vigilato MAN, Zinsstag J, Dushoff J. 2015. Estimating the global burden of endemic canine rabies. PLoS Negl Trop Dis 9:e0003709. https://doi.org/10.1371/journal.pntd.0003709.
4. Rupprecht C, Kuzmin I, Meslin F. 2017. Lyssaviruses and rabies: current conundrums, concerns, contradictions and controversies. F1000Research 6:184. https://doi.org/10.12688/f1000research.10416.1.
5. Griffin DE. 2003. Immune responses to RNA-virus infections of the CNS. Nat Rev Immunol 3:493–502. https://doi.org/10.1038/nri1105.
6. Lafon M, Megret F, Lafage M, Prehaud C. 2006. The innate immune facet of brain: human neurons express TLR-3 and sense viral dsRNA. J Mol Neurosci 29:185–194. https://doi.org/10.1385/JMN:29:3:185.
7. Hornung V, Ellegast J, Kim S, Brzozka K, Jung A, Kato H, Poeck H, Akira S, Conzelmann K-K, Schlee M, Endres S, Hartmann G. 2006. 5'-Triphosphate RNA is the ligand for RIG-I. Science 314:994–997. https://doi.org/10.1126/science.1132505.
8. Menager P, Roux P, Megret F, Bourgeois J-P, Le Sourd A-M, Danckaert A, Lafage M, Prehaud C, Lafon M. 2009. Toll-like receptor 3 (TLR3) plays a major role in the formation of rabies virus Negri Bodies. PLoS Pathog 5:e1000315. https://doi.org/10.1371/journal.ppat.1000315.
9. Chopy D, Pothlichet J, Lafage M, Megret F, Fiette L, Si-Tahar M, Lafon M. 2011. Ambivalent role of the innate immune response in rabies virus pathogenesis. J Virol 85:6657–6668. https://doi.org/10.1128/JVI.00302-11.
10. Chopy D, Detje CN, Lafage M, Kalinke U, Lafon M. 2011. The type I interferon response bridles rabies virus infection and reduces pathogenicity. J Neurovirol 17:353–367. https://doi.org/10.1007/s13365-011-0041-6.
11. Lafon M. 2008. Immune evasion, a critical strategy for rabies virus. Dev Biol (Basel) 131:413–419.
12. Hemachudha T. 1994. Human rabies: clinical aspects, pathogenesis, and potential therapy. Curr Top Microbiol Immunol 187:121–143.
13. Hooper DC, Morimoto K, Bette M, Weihe E, Koprowski H, Dietzschold B. 1998. Collaboration of antibody and inflammation in clearance of rabies virus from the central nervous system. J Virol 72:3711–3719.
14. Price RW, Brew BJ, Rosenblum M. 1990. The AIDS dementia complex and HIV-1 brain infection: a pathogenetic model of virus-immune interaction. Res Publ Assoc Res Nerv Ment Dis 68:269–290.
15. Carbone KM, Duchala CS, Narayan O. 1988. Borna disease. An immunopathologic response to viral infection in the CNS. Ann N Y Acad Sci 540:661–662.
16. Park C-H, Kondo M, Inoue S, Noguchi A, Oyamada T, Yoshikawa H, Yamada A. 2006. The histopathogenesis of paralytic rabies in six-week-old C57BL/6J mice following inoculation of the CVS-11 strain into the right triceps surae muscle. J Vet Med Sci 68:589–595. https://doi.org/10.1292/jvms.68.589.
17. Jackson AC, Reimer DL. 1989. Pathogenesis of experimental rabies in mice: an immunohistochemical study. Acta Neuropathol 78:159–165. https://doi.org/10.1007/BF00688204.
18. Coulon P, Derbin C, Kucera P, Lafay F, Prehaud C, Flamand A. 1989.

Invasion of the peripheral nervous systems of adult mice by the CVS strain of rabies virus and its avirulent derivative AvO1. J Virol 63:3550–3554.
19. Rosseels V, Naze F, De Craeye S, Francart A, Kalai M, Van Gucht S. 2011. A non-invasive intranasal inoculation technique using isoflurane anesthesia to infect the brain of mice with rabies virus. J Virol Methods 173:127–136. https://doi.org/10.1016/j.jviromet.2011.01.019.
20. Blonska M, Lin X. 2011. NF-kappaB signaling pathways regulated by CARMA family of scaffold proteins. Cell Res 21:55–70. https://doi.org/10.1038/cr.2010.182.
21. Rosebeck S, Rehman AO, Lucas PC, McAllister-Lucas LM. 2011. From MALT lymphoma to the CBM signalosome: three decades of discovery. Cell Cycle 10:2485–2496. https://doi.org/10.4161/cc.10.15.16923.
22. Juilland M, Thome M. 2016. Role of the CARMA1/BCL10/MALT1 complex in lymphoid malignancies. Curr Opin Hematol 23:402–409. https://doi.org/10.1097/MOH.0000000000000257.
23. Ekambaram P, Lee J-YL, Hubel NE, Hu D, Yerneni S, Campbell PG, Pollock N, Klei LR, Concel VJ, Delekta PC, Chinnaiyan AM, Tomlins SA, Rhodes DR, Priedigkeit N, Lee AV, Oesterreich S, McAllister-Lucas LM, Lucas PC. 2018. The CARMA3-Bcl10-MALT1 signalosome drives NFkappaB activation and promotes aggressiveness in angiotensin II receptor-positive breast cancer. Cancer Res 78:1225–1240. https://doi.org/10.1158/0008-5472.CAN-17-1089.
24. Hailfinger S, Nogai H, Pelzer C, Jaworski M, Cabalzar K, Charton J-E, Guzzardi M, Decaillet C, Grau M, Dorken B, Lenz P, Lenz G, Thome M. 2011. Malt1-dependent RelB cleavage promotes canonical NF-kappaB activation in lymphocytes and lymphoma cell lines. Proc Natl Acad Sci U S A 108:14596–14601. https://doi.org/10.1073/pnas.1105020108.
25. Staal J, Driege Y, Bekaert T, Demeyer A, Muyllaert D, Van Damme P, Gevaert K, Beyaert R. 2011. T-cell receptor-induced JNK activation requires proteolytic inactivation of CYLD by MALT1. EMBO J 30:1742–1752. https://doi.org/10.1038/emboj.2011.85.
26. Douanne T, Gavard J, Bidere N. 2016. The paracaspase MALT1 cleaves the LUBAC subunit HOIL1 during antigen receptor signaling. J Cell Sci 129:1775–1780. https://doi.org/10.1242/jcs.185025.
27. Elton L, Carpentier I, Staal J, Driege Y, Haegman M, Beyaert R. 2016. MALT1 cleaves the E3 ubiquitin ligase HOIL-1 in activated T cells, generating a dominant negative inhibitor of LUBAC-induced NF-kappaB signaling. FEBS J 283:403–412. https://doi.org/10.1111/febs.13597.
28. Jeltsch KM, Hu D, Brenner S, Zoller J, Heinz GA, Nagel D, Vogel KU, Rehage N, Warth SC, Edelmann SL, Gloury R, Martin N, Lohs C, Lech M, Stehklein JE, Geerlof A, Kremmer E, Weber A, Anders H-J, Schmitz I, Schmidt-Supprian M, Fu M, Holtmann H, Krappmann D, Ruland J, Kallies A, Heikenwalder M, Heissmeyer V. 2014. Cleavage of roquin and regnase-1 by the paracaspase MALT1 releases their cooperatively repressed targets to promote T(H)17 differentiation. Nat Immunol 15:1079–1089. https://doi.org/10.1038/ni.3008.
29. Uehata T, Iwasaki H, Vandenbon A, Matsushita K, Hernandez-Cuellar E, Kuniyoshi K, Satoh T, Mino T, Suzuki Y, Standley DM, Tsujimura T, Rakugi H, Isaka Y, Takeuchi O, Akira S. 2013. Malt1-induced cleavage of regnase-1 in CD4(+) helper T cells regulates immune activation. Cell 153:1036–1049. https://doi.org/10.1016/j.cell.2013.04.034.
30. Afonina IS, Elton L, Carpentier I, Beyaert R. 2015. MALT1—a universal soldier: multiple strategies to ensure NF-kappaB activation and target gene expression. FEBS J 282:3286–3297. https://doi.org/10.1111/febs.13325.
31. Ruefli-Brasse AA, French DM, Dixit VM. 2003. Regulation of NF-kappaB-

dependent lymphocyte activation and development by paracaspase. Science 302:1581–1584. https://doi.org/10.1126/science.1090769.

32. Ruland J, Duncan GS, Wakeham A, Mak TW. 2003. Differential requirement for Malt1 in T and B cell antigen receptor signaling. Immunity 19:749–758. https://doi.org/10.1016/S1074-7613(03)00293-0.

33. Demeyer A, Staal J, Beyaert R. 2016. Targeting MALT1 proteolytic activity in immunity, inflammation and disease: good or bad? Trends Mol Med 22:135–150. https://doi.org/10.1016/j.molmed.2015.12.004.

34. Mc Guire C, Wieghofer P, Elton L, Muylaert D, Prinz M, Beyaert R, van Loo G. 2013. Paracaspase MALT1 deficiency protects mice from autoimmune-mediated demyelination. J Immunol 190:2896–2903. https://doi.org/10.4049/jimmunol.1201351.

35. Mc Guire C, Elton L, Wieghofer P, Staal J, Voet S, Demeyer A, Nagel D, Krappmann D, Prinz M, Beyaert R, van Loo G. 2014. Pharmacological inhibition of MALT1 protease activity protects mice in a mouse model of multiple sclerosis. J Neuroinflammation 11:124. https://doi.org/10.1186/1742-2094-11-124.

36. Lee CH, Bae SJ, Kim M. 2017. Mucosa-associated lymphoid tissue lymphoma translocation 1 as a novel therapeutic target for rheumatoid arthritis. Sci Rep 7:11889. https://doi.org/10.1038/s41598-017-12349-9.

37. Nakamura Y, Yokoyama K, Igaki K, Tsuchimori N. 2018. Role of Malt1 protease activity in pathogenesis of inflammatory disorders mediated by FcgammaR signaling. Int Immunopharmacol 56:193–196. https://doi.org/10.1016/j.intimp.2018.01.028.

38. Fontan L, Yang C, Kabaleeswaran V, Volpon L, Osborne MJ, Beltran E, Garcia M, Cerchietti L, Shaknovich R, Yang SN, Fang F, Gascoyne RD, Martinez-Climent JA, Glickman JF, Borden K, Wu H, Melnick A. 2012. MALT1 small molecule inhibitors specifically suppress ABC-DLBCL in vitro and in vivo. Cancer Cell 22:812–824. https://doi.org/10.1016/j.ccr.2012.11.003.

39. Nagel D, Spranger S, Vincendeau M, Grau M, Raffegerst S, Kloo B, Hlahla D, Neuenschwander M, Peter von Kries J, Hadian K, Dorken B, Lenz P, Lenz G, Schendel DJ, Krappmann D. 2012. Pharmacologic inhibition of MALT1 protease by phenothiazines as a therapeutic approach for the treatment of aggressive ABC-DLBCL. Cancer Cell 22:825–837. https://doi.org/10.1016/j.ccr.2012.11.002.

40. Schlauderer F, Lammens K, Nagel D, Vincendeau M, Eitelhuber AC, Verhelst SHL, Kling D, Chrusciel A, Ruland J, Krappmann D, Hopfner K-P. 2013. Structural analysis of phenothiazine derivatives as allosteric inhibitors of the MALT1 paracaspase. Angew Chem Int Ed Engl 52:10384–10387. https://doi.org/10.1002/anie.201304290.

41. Bardet M, Unterreiner A, Malinverni C, Lafossas F, Vedrine C, Boesch D, Kolb Y, Kaiser D, Gluck A, Schneider MA, Katopodis A, Renatus M, Simic O, Schlapbach A, Quancard J, Regnier CH, Bold G, Pissot-Soldermann C, Carballido JM, Kovarik J, Calzascia T, Bornancin F. 2018. The T-cell fingerprint of MALT1 paracaspase revealed by selective inhibition. Immunol Cell Biol 96:81–99. https://doi.org/10.1111/imcb.1018.

42. Fu ZF, Jackson AC. 2005. Neuronal dysfunction and death in rabies virus infection. J Neurovirol 11:101–106. https://doi.org/10.1080/13550280590900445.

43. Scott CA, Rossiter JP, Andrew RD, Jackson AC. 2008. Structural abnormalities in neurons are sufficient to explain the clinical disease and fatal outcome of experimental rabies in yellow fluorescent protein-expressing transgenic mice. J Virol 82:513–521. https://doi.org/10.1128/JVI.01677-07.

44. Torres-Anjel MJ, Volz D, Torres MJ, Turk M, Tshikuka JG. 1988. Failure to thrive, wasting syndrome, and immunodeficiency in rabies: a hypophyseal/hypothalamic/thymic axis effect of rabies virus. Rev Infect Dis 10(Suppl 4):S710–S725. https://doi.org/10.1093/clinids/10.Supplement_4.S710.

45. Zhao L, Toriumi H, Kuang Y, Chen H, Fu ZF. 2009. The roles of chemokines in rabies virus infection: overexpression may not always be beneficial. J Virol 83:11808–11818. https://doi.org/10.1128/JVI.01346-09.

46. Laothamatas J, Wacharapluesadee S, Lumlertdacha B, Ampawong S, Tepsumethanon V, Shuangshoti S, Phumesin P, Asavaphatiboon S, Worapruekjaru L, Avihingsanon Y, Israsena N, Lafon M, Wilde H, Hemachudha T. 2008. Furious and paralytic rabies of canine origin: neuroimaging with virological and cytokine studies. J Neurovirol 14:119–129. https://doi.org/10.1080/13550280701883857.

47. Wang ZW, Sarmento L, Wang Y, Li X, Dhingra V, Tseggai T, Jiang B, Zhen F, Fu ZF. 2005. Attenuated rabies virus activates, while pathogenic rabies virus evades, the host innate immune responses in the central nervous system attenuated rabies virus activates, while pathogenic rabies virus evades, the host innate immune responses in the central nervous system. J Virol 79:12554–12565. https://doi.org/10.1128/JVI.79.19.12554-12565.2005.

48. Brustle A, Brenner D, Knobbe CB, Lang PA, Virtanen C, Hershenfield BM, Reardon C, Lacher SM, Ruland J, Ohashi PS, Mak TW. 2012. The NF-kappaB regulator MALT1 determines the encephalitogenic potential of Th17 cells. J Clin Invest 122:4698–4709. https://doi.org/10.1172/JCI63528.

49. Johnson N, Mansfield KL, Hicks D, Nunez A, Healy DM, Brookes SM, McKimmie C, Fazakerley JK, Fooks AR. 2008. Inflammatory responses in the nervous system of mice infected with a street isolate of rabies virus. Dev Biol (Basel) 131:65–72.

50. Baloul L, Lafon M. 2003. Apoptosis and rabies virus neuroinvasion. Biochimie 85:777–788. https://doi.org/10.1016/S0300-9084(03)00137-8.

51. Fernandes ER, de Andrade HFJ, Lancellotti CLP, Quaresma JAS, Demachki S, da Costa Vasconcelos PF, Duarte MIS. 2011. In situ apoptosis of adaptive immune cells and the cellular escape of rabies virus in CNS from patients with human rabies transmitted by Desmodus rotundus. Virus Res 156:121–126. https://doi.org/10.1016/j.virusres.2011.01.006.

52. Hooper DC, Roy A, Barkhouse DA, Li J, Kean RB. 2011. Rabies virus clearance from the central nervous system. Adv Virus Res 79:55–71. https://doi.org/10.1016/B978-0-12-387040-7.00004-4.

53. Lafon M. 2011. Evasive strategies in rabies virus infection. Adv Virus Res 79:33–53. https://doi.org/10.1016/B978-0-12-387040-7.00003-2.

54. Kip E, Staal J, Verstrepen L, Tima HG, Terryn S, Romano M, Lemeire K, Suin V, Hamouda A, Kalai M, Beyaert R, Van Gucht S. 2018. MALT1 controls attenuated rabies virus by inducing early inflammation and T cell activation in the brain. J Virol 92:e02029-17. https://doi.org/10.1128/JVI.02029-17.

55. Wang T, Town T, Alexopoulou L, Anderson JF, Fikrig E, Flavell RA. 2004. Toll-like receptor 3 mediates West Nile virus entry into the brain causing lethal encephalitis. Nat Med 10:1366–1373. https://doi.org/10.1038/nm1140.

56. Gross O, Poeck H, Bscheider M, Dostert C, Hannesschläger N, Endres S, Hartmann G, Tardivel A, Schweighoffer E, Tybulewicz V, Mocsai A, Tschopp J, Ruland J. 2009. Syk kinase signalling couples to the Nlrp3 inflammasome for anti-fungal host defence. Nature 459:433–436. https://doi.org/10.1038/nature07965.

57. Jiang C, Zhou Z, Quan Y, Zhang S, Wang T, Zhao X, Morrison C, Heise MT, He W, Miller MS, Lin X. 2016. CARMA3 is a host factor regulating the balance of inflammatory and antiviral responses against viral infection. Cell Rep 14:2389–2401. https://doi.org/10.1016/j.celrep.2016.02.031.

58. Clausen BE, Burkhardt C, Reith W, Renkawitz R, Forster I. 1999. Conditional gene targeting in macrophages and granulocytes using LysMcre mice. Transgenic Res 8:265–277. https://doi.org/10.1023/A:1008942828960.

59. Kojima D, Park C-H, Satoh Y, Inoue S, Noguchi A, Oyamada T. 2009. Pathology of the spinal cord of C57BL/6J mice infected with rabies virus (CVS-11 strain). J Vet Med Sci 71:319–324. https://doi.org/10.1292/jvms.71.319.

60. Michel PP, Hirsch EC, Agid Y. 2002. Parkinson disease: mechanisms of cell death. Rev Neurol (Paris) 158(Spec no 1):S24–S32. (In French.)

61. Garden GA. 2002. Microglia in human immunodeficiency virus-associated neurodegeneration. Glia 40:240–251. https://doi.org/10.1002/glia.10155.

62. Rogove AD, Lu W, Tsirka SE. 2002. Microglial activation and recruitment, but not proliferation, suffice to mediate neurodegeneration. Cell Death Differ 9:801–806. https://doi.org/10.1038/sj.cdd.4401041.

63. Ferencik M, Novak M, Rovensky J, Rybar I. 2001. Alzheimer's disease, inflammation and non-steroidal anti-inflammatory drugs. Bratisl Lek Listy 102:123–132.

64. Wolf J, Yona S, Kim K-W, Jung S. 2013. Microglia, seen from the CX3CR1 angle. Front Cell Neurosci 7:26. https://doi.org/10.3389/fncel.2013.00026.

65. Jeohn GH, Kong LY, Wilson B, Hudson P, Hong JS. 1998. Synergistic neurotoxic effects of combined treatments with cytokines in murine primary mixed neuron/glia cultures. J Neuroimmunol 85:1–10. https://doi.org/10.1016/S0165-5728(97)00204-X.

66. Meda L, Cassatella MA, Szendrei GI, Otvos LJ, Baron P, Villalba M, Ferrari D, Rossi F. 1995. Activation of microglial cells by beta-amyloid protein and interferon-gamma. Nature 374:647–650. https://doi.org/10.1038/374647a0.

67. Camelo S, Lafage M, Lafon M. 2000. Absence of the p55 Kd TNF-alpha receptor promotes survival in rabies virus acute encephalitis. J Neurovirol 6:507–518. https://doi.org/10.3109/13550280009091951.

68. Smreczak M, Marzec A, Orlowska A, Trebas P, Reichert M, Kycko A, Koraka P, Osterhaus A, Zmudzinski JF. 2017. The effect of selected

molecules influencing the detrimental host immune response on a course of rabies virus infection in a murine model. Vaccine https://doi.org/10.1016/j.vaccine.2017.10.098.

69. Kip E, Naze F, Suin V, Vanden Berghe T, Francart A, Lamoral S, Vandenabeele P, Beyaert R, Van Gucht S, Kalai M. 2017. Impact of caspase-1/11, -3, -7, or IL-1beta/IL-18 deficiency on rabies virus-induced macrophage cell death and onset of disease. Cell Death Discov 3:17012. https://doi.org/10.1038/cddiscovery.2017.12.

70. Hooper DC, Ohnishi ST, Kean R, Numagami Y, Dietzschold B, Koprowski H. 1995. Local nitric oxide production in viral and autoimmune diseases of the central nervous system. Proc Natl Acad Sci U S A 92:5312–5316.

71. Madhu BP, Singh KP, Saminathan M, Singh R, Tiwari AK, Manjunatha V, Harish C, Manjunathareddy GB. 2016. Correlation of inducible nitric oxide synthase (iNOS) inhibition with TNF-alpha, caspase-1, FasL and TLR-3 in pathogenesis of rabies in mouse model. Virus Genes 52:61–70. https://doi.org/10.1007/s11262-015-1265-y.

72. Koprowski H, Zheng YM, Heber-Katz E, Fraser N, Rorke L, Fu ZF, Hanlon C, Dietzschold B. 1993. In vivo expression of inducible nitric oxide synthase in experimentally induced neurologic diseases. Proc Natl Acad Sci U S A 90:3024–3027.

73. Ubol S, Sukwattanapan C, Maneerat Y. 2001. Inducible nitric oxide synthase inhibition delays death of rabies virus-infected mice. J Med Microbiol 50:238–242. https://doi.org/10.1099/0022-1317-50-3-238.

74. Nakamichi K, Inoue S, Takasaki T, Morimoto K, Kurane I. 2004. Rabies virus stimulates nitric oxide production and CXC chemokine ligand 10 expression in macrophages through activation of extracellular signal-regulated kinases 1 and 2. J Virol 78:9376–9388. https://doi.org/10.1128/JVI.78.17.9376-9388.2004.

75. Narni-Mancinelli E, Chaix J, Fenis A, Kerdiles YM, Yessaad N, Reynders A, Gregoire C, Luche H, Ugolini S, Tomasello E, Walzer T, Vivier E. 2011. Fate mapping analysis of lymphoid cells expressing the NKp46 cell surface receptor. Proc Natl Acad Sci U S A 108:18324–18329. https://doi.org/10.1073/pnas.1112064108.

76. Office International des Epizooties. 2018. Manual of diagnostic tests and vaccines for terrestrial animals, 8th ed, p 14 to 20. Office International des Epizooties, Paris, France.

77. Pösel C, Möller K, Boltze J, Wagner D-C, Weise G. 2016. Isolation and flow cytometric analysis of immune cells from the ischemic mouse brain. J Vis Exp 2016:53658. https://doi.org/10.3791/53658.